

Aerosol aware data assimilation system: The response of CRTM simulation and GSI analysis to the presence of aerosols

Project Report for 2019 DTC Visitor Program

Shih-Wei Wei

University at Albany, State University of New York, Albany, NY

Email: S.-W. Wei (swei@albany.edu)

1. Background and Introduction

Aerosol radiative effects, both direct and indirect, have been extensively studied using climate and numerical weather prediction (NWP) models. However, the aerosol impacts on radiance in the context of data assimilation (DA) have received less research attention. The thermal infrared (IR) radiance observations have been assimilated since the mid-1990s. Many studies have demonstrated a pronounced deduction in brightness temperature (BT) simulations at the IR window channels due to the presence of aerosols (Sokolik, 2002; Weaver et al., 2003; Pierangelo et al., 2004; Matricardi, 2005; Liu et al., 2007; Chen et al., 2012; Quan et al., 2013; Kim et al., 2018). Moreover, the quality of IR observation retrievals can be improved by considering aerosol radiative effects. Merchant et al. (2006) indicated that the bias of the sea surface temperature (SST) retrieval can be reduced with proper estimation of dust aerosol impacts on IR observations. Divakarla et al. (2012) reported that the temperature retrievals of IR sounder have less deviation from reanalysis when the dust contaminated observations were removed.

Clear-sky IR observations are assimilated in modern DA systems. For instance, the Gridpoint Statistical Interpolation (GSI) rejects IR observations affected by clouds (Liang and Weng, 2014). However, the aerosol-affected observations are not explicitly identified and rejected in the quality control (QC) algorithm. It implies that aerosol-affected IR observations can be either assimilated like clear-sky observations or rejected like cloudy-sky observations. Moreover, aerosol information is not considered in the BT simulation by the radiance observation operator. In this case, assimilating aerosol-affected IR observations can introduce anomalous cooling into the GSI analysis.

In the GSI, the Community Radiative Transfer Model (CRTM) is the radiance observation operator which has the capability to simulate the multiple-scattering process of aerosols and clouds. CRTM was developed at the Joint Center for Satellite Data Assimilation (JCSDA) with contributions from NOAA scientists (Weng et al., 2005; Han et al., 2006). In terms of the CRTM aerosol module (Liu and Lu, 2016), the specification of aerosol optical properties is based on the Goddard Chemistry Aerosol Radiation and Transport (GOCART; Chin et al., 2000; Colarco et al. 2010) model. To exploit the aerosol-affected IR observations in the GSI, it is necessary to understand the response of the BT forward operator and its Jacobians in the CRTM to the presence of aerosols. Furthermore, it is desired to investigate the impacts of aerosol-affected BTs and Jacobians on the analysis.

2. Methods

A series of sensitivity tests based on CRTM version 2.3.0 is conducted to investigate the response of simulated BTs and Jacobians to the aerosol optical and geometrical properties. The U.S. Standard Atmosphere profiles of temperature and water vapor mixing ratio are used. Among GOCART aerosol species, dust aerosols generate the largest cooling effects on BTs (Kim et al., 2018). Hence, we focused on dust aerosols in this study. The dust aerosol profiles are produced by an artificial formulation that is inferred from the climatology of Modern-Era Retrospective Analysis for Research and Applications, Version 2 (MERRA-2) and the near real-time analysis of Goddard Earth Observing System (GEOS) forward processing (FP) in June 2020.

The reference dust profile is generated with column mass density of $1.967 \times 10^{-3} \text{ kg m}^{-2}$ (550 nm AOD ~ 0.9) to represent a location near the source region. The dust layer peaks around 500 hPa and majorly distributes between 487 and 718 hPa. The thickness of the dust layer is defined by the layers which have dust mass density over 80% of the mass density at peak layer. Five bins of GOCART dust aerosols are considered in the CRTM. The effective radius of each bin is 0.55, 1.4, 2.4, 4.5, and 8.0 μm , respectively. Each bin occupies 10%, 40%, 30%, 15%, and 5% of the total loading in the reference profile.

Figures 1 and 2 show the perturbed dust profiles applied in the experiments. These include profiles that vary in AOD, peak level, and thickness of the aerosol layer (Figure 1). In

addition, sensitivity tests for bin partition were conducted with changing the bin partitions of the reference profile to 15%, 45%, 35%, 5%, and 0% to represent a profile in an area downwind (Figure 2b). Except for the sensitivity test of the column mass density, the dust loading is fixed to the reference profile ($1.967 \times 10^{-3} \text{ kg m}^{-2}$) in these tests. The BT simulation and Jacobians are then assessed under the different sets of sensitivity tests. The entire spectral range of the Infrared Atmospheric Sounding Interferometer (IASI) is selected to perform the sensitivity tests due to its high spectral resolution (0.5 cm^{-1}) and wide coverage ($645 \text{ to } 2760 \text{ cm}^{-1}$).

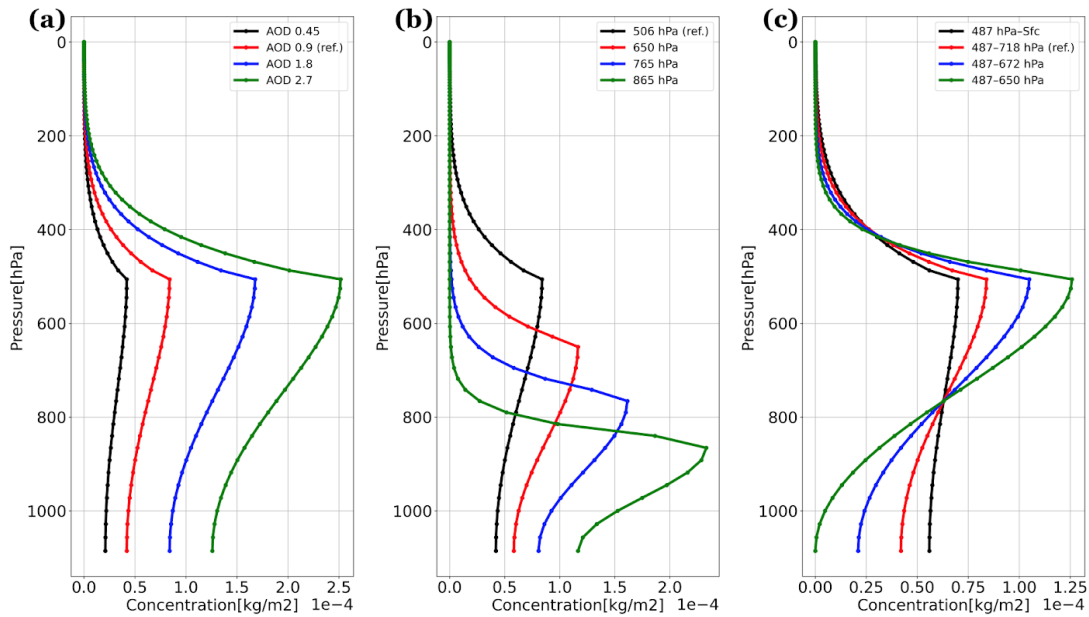


Figure 1. The perturbation dust profiles for our sensitivity tests, which vary in column mass density (a), altitude of peak dust layer (b), and thickness (c). The reference profile is also labeled in (a – c).

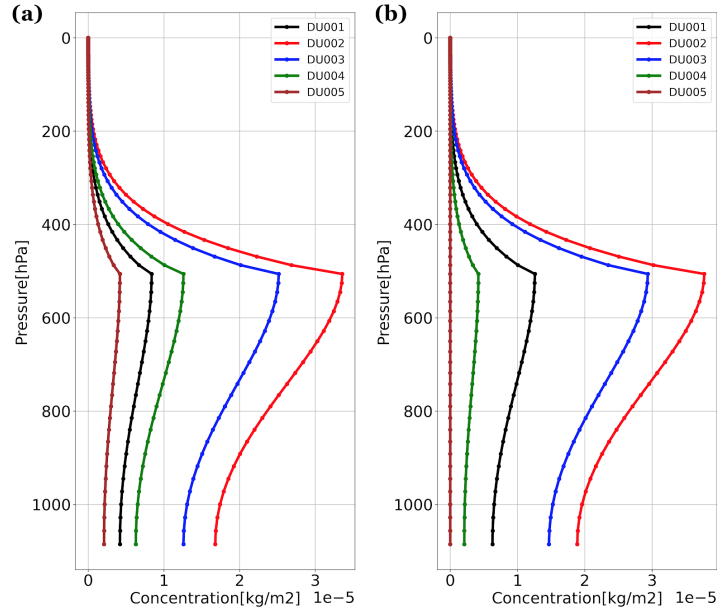


Figure 2. The perturbation of dust bin partitions for the (a) reference profile and (b) perturbed profile. The bin partitions of the reference profile are used in this sensitivity test.

In addition to the CRTM sensitivity tests, two standalone GSI experiments on 12Z June 22, 2020 were conducted to demonstrate the impacts of aerosol-affected BTs and Jacobians on the analysis. These include: (1) the aerosol-blind run (noted as CTL later), which is the baseline GSI, and (2) the aerosol-aware run (noted as AER later). Both experiments use the same observational dataset, but the aerosol radiative effects are considered in the BT simulations of the IR sensors in AER. The corresponding time-varying three-dimensional aerosol information from MERRA-2 is incorporated into the CRTM simulation.

3. Results

3.1 Sensitivity of BT Simulations

Figure 3a shows the stimulated BTs under clear-sky (labeled as Ctl) and hazy-sky with reference dust profile (labeled as Ref) and Figure 3b shows their differences. It is shown that when dust aerosols were considered in the CRTM simulation, the BTs decreased by about 10 K in the longwave IR window, 5 K at 750 to 900 cm^{-1} , and about 2 K in the shortwave IR window. This cooling effect has a similar spectral behavior to the results from Matricardi (2005) and Kim et al. (2018) but with different magnitudes, which is expected given the different aerosol loading.

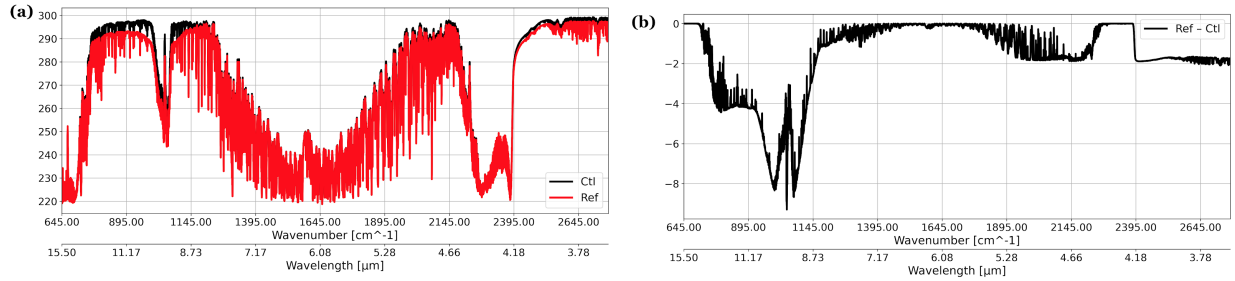


Figure 3. The comparison of brightness temperature simulation for IASI from (a) clear-sky (black) and the reference dust profile (red) and (b) the difference (Ref – Ctl).

Figure 4 displays the relative change of BT with respect to the reference for the four sensitivity tests illustrated in Figures 1 and 2. In the perturbation of column mass density (Figure 1a), the loading is perturbed by -50%, +100%, and +200% of the reference state. Figure 4a shows that the cooling effect in simulated BTs is weakened by about 5 K under half the amount of mass density in the reference profile. It is about half of the BT cooling in the reference case (Figure 3b). In the longwave IR window, there is an additional 7.5 K cooling effect when double the dust loading; while additional 15 K when the loading is tripled. This is expected as the aerosol layer with larger loading is optically thicker and thus blocks more IR radiation emitted from the surface.

For the experiments investigating the sensitivity to the aerosol peak level, the column-integrated dust loading is the same as the reference profile, as mentioned above. The altitude of the peak dust layer descends from 500 hPa (reference profile) to 650 hPa, 750 hPa, and 850 hPa (Figure 1b). Figure 4b shows that the magnitude of cooling effect decreases as the peak level lowers in altitude. The cooling effect reduces by about 3.5 K for the dust layer that peaks at 850 hPa. This feature implies that the aerosol layer confined in the lower level has smaller impacts on BT. It is consistent with the findings in Pierangelo et al. (2004). This may be due to the BT simulation becoming more sensitive to the temperature of the aerosol layer, which is warmer in lower atmosphere (i.e., 850 hPa case). So the dust layer peaked at lower altitude would emit stronger IR radiation to the top of the atmosphere than the dust layer peaked at higher altitude.

Regarding the sensitivity to the dust layer thickness, the profile is perturbed by the ratio of loading between peak layer and surface. Since the column mass density is fixed, the peak

loading is different between each perturbed profile (Figure 1c). As a result, the layer thickness varied from 487–718 hPa (reference) to 487–650 hPa, 487–672 hPa, and 487 hPa–surface. Figure 4c shows the cooling effect becomes smaller when the dust layer is thicker (i.e., 487 hPa–surface). When the dust aerosols are confined to the mid-atmosphere (i.e., 487–650 hPa) the cooling effect is strengthened by about 0.6 K. This indicates that larger mass density in a more confined layer could result in a stronger cooling effect under the same loading.

For the sensitivity test for the bins partition, the coarser bin (i.e., DU005) is removed to represent the dust profile over the downwind region (Figure 2b), such as the Caribbean Sea. Figure 4d indicates that the BT at longwave IR window channels are cooler by about 0.8K, assuming the same column mass density. This implies that the more fine bin dust particles leads to a stronger cooling effect.

Overall the four sensitivity tests indicate that the column mass density and the altitude of peak dust layer are the primary and secondary factors affecting the BT simulation, respectively. The magnitude of changes due to aerosol layer thickness and bins partition is relatively small. Both are less than 1K while 15K in the case of column mass density and 3.5K in the case of peak altitude.

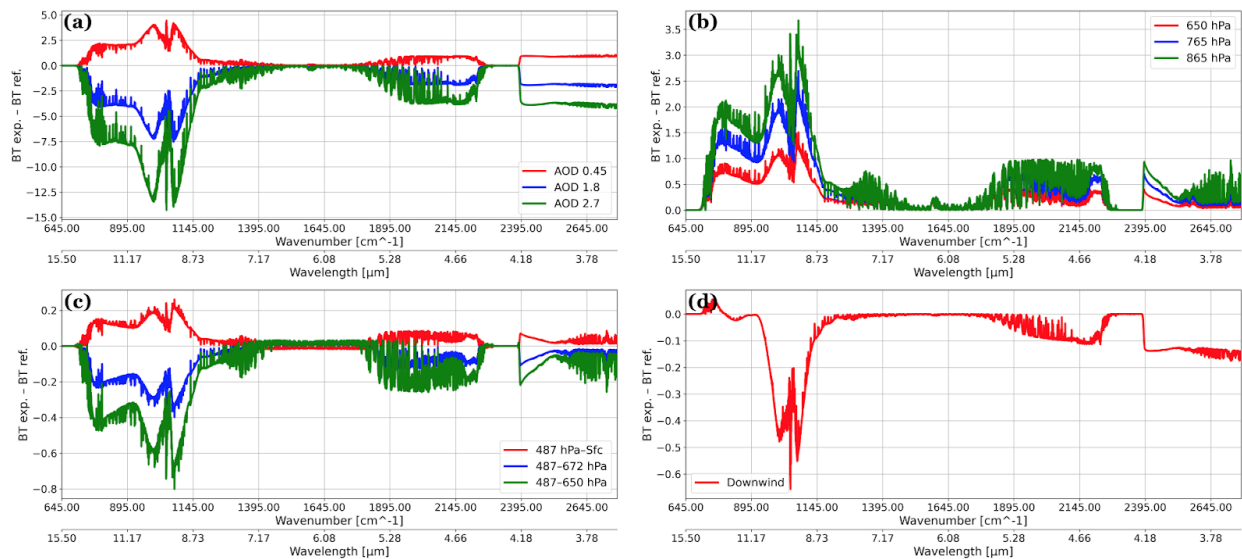


Figure 4. The relative change of brightness temperature simulation of IASI against the reference dust profile for each sensitivity test: (a) column mass density, (b) altitude of peak dust layer, (c) thickness, and (d) bins partition.

3.2 Sensitivity of BT Jacobians

In this section, we examine the BT Jacobians for the layer temperature (J_T), water vapor (J_Q), surface temperature (J_{Ts}) and surface emissivity (J_ϵ). To quantify the changes of the BT Jacobian in the CRTM simulation, the approach of goodness of fit measure (M) in Garand et al. (2001) is applied. The M value can be calculated through the equation below,

$$M = 100 \sqrt{\frac{\sum_{l=1}^k (J_l^m - J_l^r)^2}{\sum_{l=1}^k (J_l^r)^2}}$$

where J^m is the Jacobian profile to evaluate, J^r is the reference Jacobian profile, and the subscript l is for the vertical layer. The J^r use the Jacobian from clear-sky. It represents the total column change rate of the Jacobian. The sensitivity of the J_T and J_Q to the perturbed dust profiles are examined by the M value; J_{Ts} and J_ϵ are directly compared to the results of clear-sky.

Figure 5 illustrates the M values of J_T and J_Q from each sensitivity test over the whole spectral domain on IASI; we exclude the results from the dust bin partitions because differences are negligible. Similar to the results of the BT simulation, the M values of J_T and J_Q also show larger sensitivity to the aerosol loading (Figure 5a and 5b) and peak level altitude (Figure 5c and 5d). The larger dust column mass density and lower peak level altitude introduce stronger changes in J_T and J_Q . Regarding the sensitivity to the dust layer thickness (Figure 5e and 5f), both the M values of J_T and J_Q show the opposite behaviors in the longwave and shortwave IR window. The M values of J_T show larger (smaller) change rates at the longwave (shortwave) IR window with the thinnest dust layer (487–650 hPa). In contrast, the M values of J_Q show the smaller (larger) change rates at the longwave (shortwave) IR window with the thinnest dust layer (487–650 hPa). Since the M value is a column integral quantity, further investigation on vertical distribution of J_T and J_Q at both IR window channels is desired.

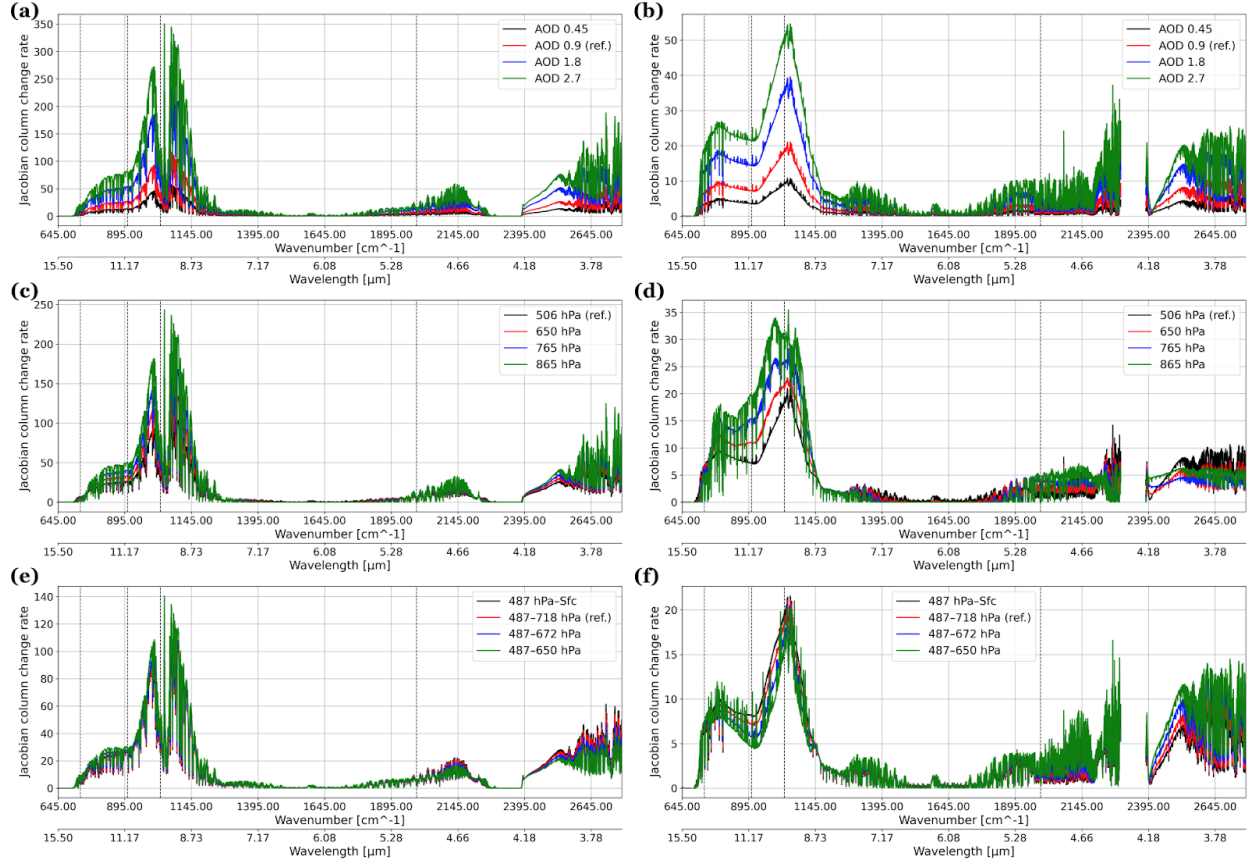


Figure 5. The column change rate of Jacobians for layer temperature (left column) and layer water vapor (right column) from sensitivity tests in (a, b) column mass density, (c, d) altitude of peak dust layer, and (e, f) thickness. The four assimilated channels are marked by dashed lines.

To demonstrate the relationship between J_T and J_Q , under the hazy-sky condition, four assimilated channels with smaller observation error assignment in the GSI are selected. Figure 6 displays the scatter plots for the sensitivity tests to the dust loading. Each layer of J_T in the x-axis and J_Q in the y-axis are plotted. In principle, considering dust aerosol information results in the larger magnitude of J_T at mid-atmosphere but smaller J_T in the lower atmosphere, while J_Q has smaller magnitude in most layers. It implies that the BT simulation of CRTM is more sensitive to the mid-level temperature and less sensitive to water vapor when aerosols are present. The vertical distribution change of the Jacobian would further affect the analysis increment in GSI. Some preliminary results are presented in Section 3.3.

It should be noted that Figure 6c demonstrates a different behavior of the J_T below 500 hPa under the heavy dust loading condition (AOD 2.7) at 1028.75 cm⁻¹ (in ozone absorption line). The J_T peaks at a similar altitude that the dust layer has the largest loading (506 hPa) and

reduces in the layers below while the other two cases show the J_T peaks at the lowest layer. It implies that the dust layer with AOD 2.7 blocks most IR radiation emitted from the layers below. This feature also suggests that BT simulation would be most sensitive to the temperature of the aerosol layer when the layer mass density is over some critical amount. However, exploring the critical value of layer mass density is beyond the scope of the present study.

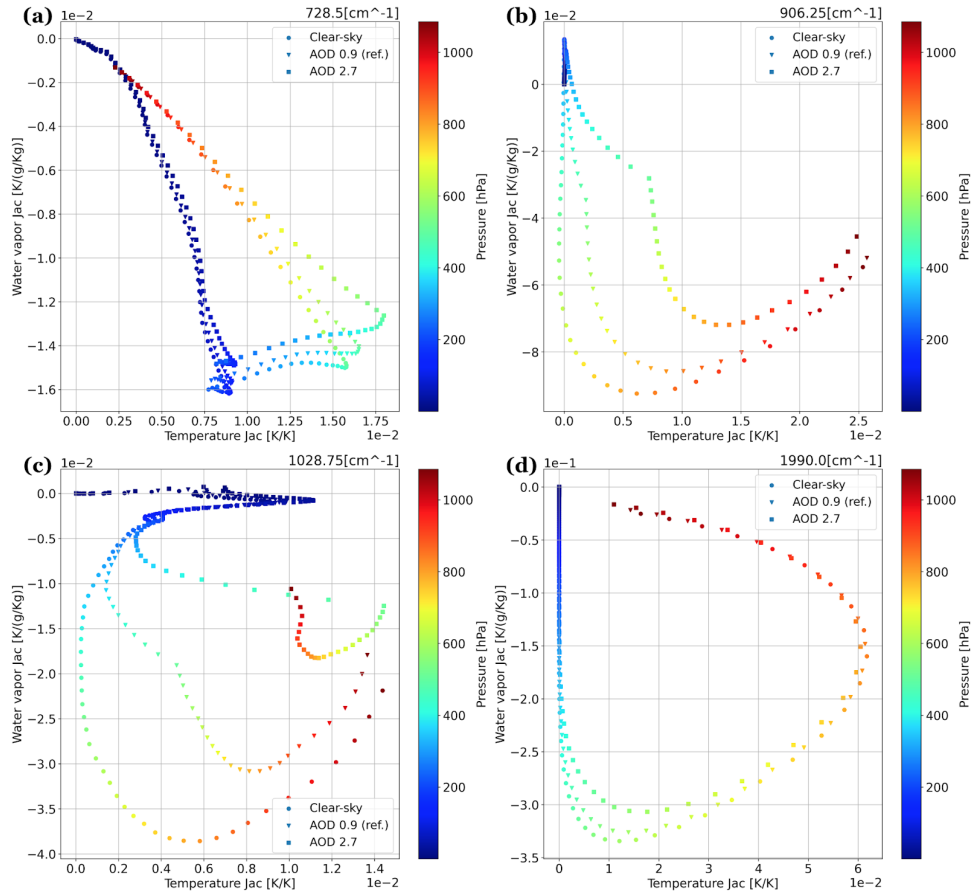


Figure 6. The scatter plots of Jacobians for layer temperature (in x) and layer water vapor (in y) from the four assimilated channels: (a) 728.5 cm^{-1} (CO_2), (b) 906.25 cm^{-1} (window), (c) 1028.75 cm^{-1} (O_3), and (d) 1990.0 cm^{-1} (H_2O). The sensitivity tests of column mass density are shown, clear-sky in \bullet , reference in \blacktriangledown , and triple loading in \blacksquare . Color of dots represents the layer pressure.

Regarding the J_{T_s} and J_{ϵ} , Figure 7 displays the comparison of BT J_{T_s} (a, b) and J_{ϵ} (c, d) between clear-sky and reference dust profile (a, c) and its sensitivity to the column mass density (b, d); differences in other sensitivity tests are not pronounced and thus excluded. Figure 7a indicates that the J_{T_s} is smaller when considering the dust aerosols. Figure 7b depicts that the J_{T_s}

decreased more when the dust loading is heavier. This implies that the BT simulation is less sensitive to the surface temperature when more IR radiation is attenuated by the dust aerosols aloft. Figure 7c shows that the J_e flips from positive to negative values when considering dust aerosols in the CRTM simulation. Figure 7d displays a very small difference between each loading. This means that the simulated BT will be cooler when the surface emissivity is increased under hazy conditions. Since the J_e is a predictor in the bias correction scheme of the GSI, more investigation is required to explore the impacts on bias correction and the usage of aerosol-affected IR observations.

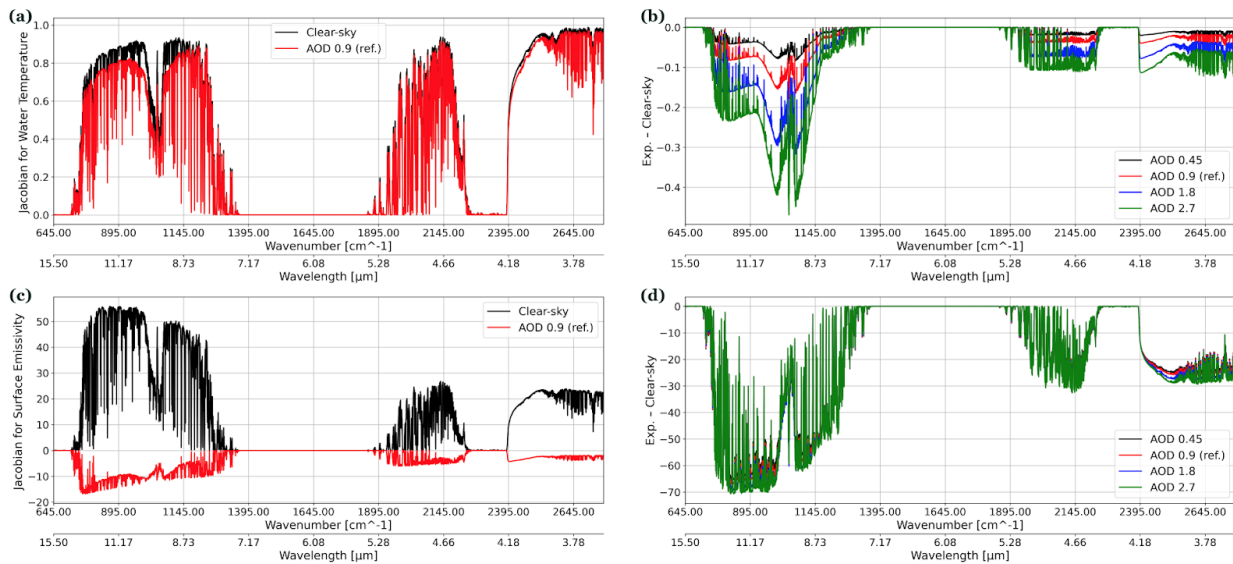


Figure 7. (a) The comparison of the Jacobian for surface temperature between clear-sky (black) and reference dust profile (red) and the (b) relative changes due to the perturbed column mass density. (c) and (d) are the same as (a) and (b) but for the results of the Jacobian for surface emissivity.

3.3 Standalone GSI experiments

Figure 8 shows (a) the analyzed temperature difference at 900 hPa between two experiments and (b) the total column mass density of the MERRA-2 aerosols incorporated in the GSI/CRTM system. The analyzed temperature differences reveal that when aerosol effects are considered in the derivation of the simulated BTs, the air temperatures are adjusted across the globe. Primarily, the AER run shows a 0.5 to 1 degree warmer analyzed temperature over the trans-Atlantic region that is heavily affected by dust. It also shows differences over the Southern Ocean where the aerosol loading is small. As shown in Figure 8, aerosol impacts would not only

affect the analysis over the aerosol-laden region but also other distant areas. The impact on dust-free regions could be attributed to the change in the contribution of IR radiances in the cost function.

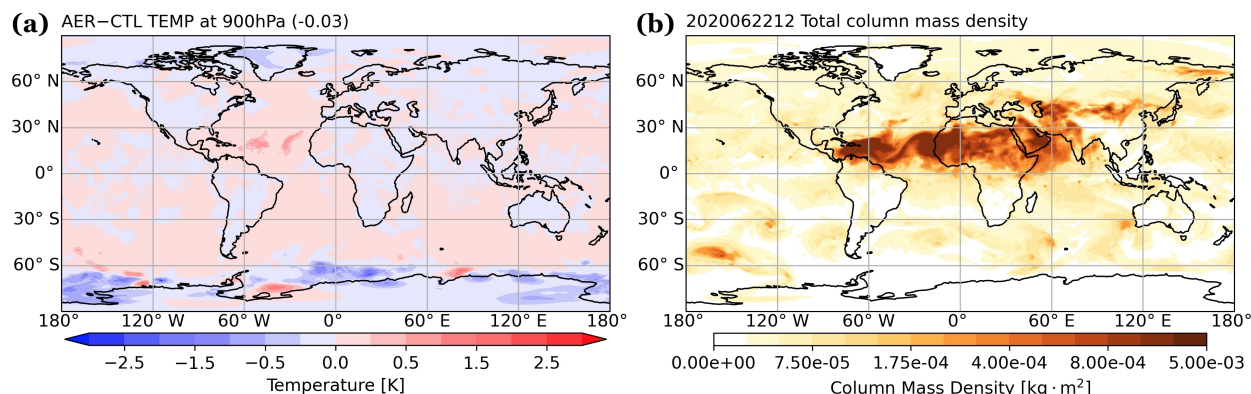


Figure 8. (a) Temperature analysis difference at 900 hPa between the AER (aerosol-aware) and the CTL (aerosol-blind) run and (b) the aerosol total column mass density (kg m^{-2}) from MERRA-2 on 12Z June 22, 2020.

Figure 9 displays the differences in the simulated BTs and first-guess departures at $10.39 \mu\text{m}$ of IASI onboard MetOp-A between the two experiments. It shows evident cooling (~ 4 to 5 K) attributed to taking aerosol information into account in CRTM (Figure 9a). Over the trans-Atlantic region, AER assimilates several observations with larger first-guess departures (Figure 9b). It contributes to the warmer analyzed temperature shown in Figure 8a. When considering aerosol information, the root-mean-square first-guess departures also decrease 0.1 K globally and 0.2 K over the trans-Atlantic region at this channel. This implies that BT simulations in AER are in better agreement with observations.

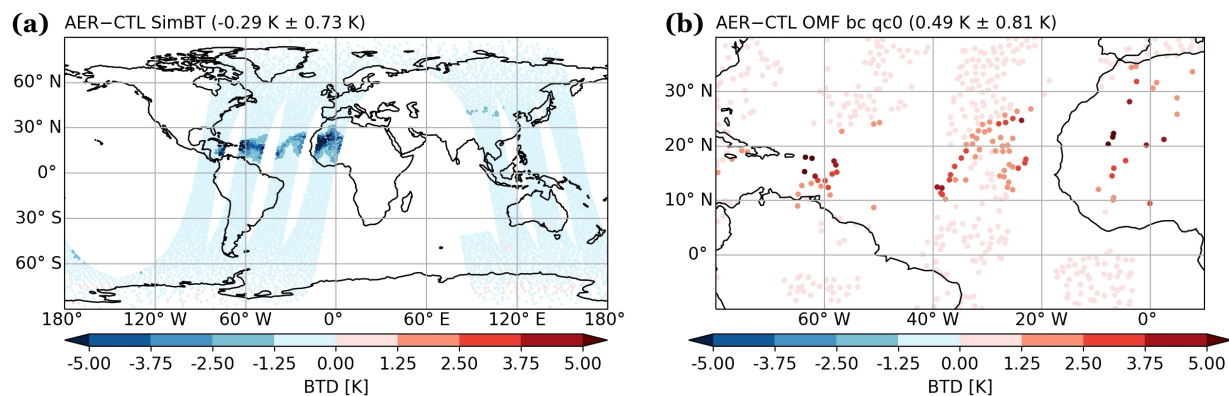


Figure 9. (a) Simulated BT and (b) first-guess departures differences (AER minus CTL) for $10.39\ \mu\text{m}$ of IASI onboard METOP-A. All the data are from the analysis cycle on 12Z June 22, 2020.

4. Regression Test

To assure the functionality of aerosol-aware BT derivations in GSI/CRTM, a regression test (“global_C96_fv3aerorad”) is added to the current GSI regression test suite. This regression test applies the same first-guess files as the regression test for aerosol DA (“global_C96_fv3aero”), which performs the aerosol analysis using satellite aerosol optical depth (AOD) observations on 00Z Jun 22, 2019. The first-guess files are taken from the aerosol member of the Global Ensemble Forecast System (GEFS-Aerosol v12; the FV3 dynamical core Unified Forecast System coupled with GOCART aerosol module). The aerosol fields in the first-guess files provide the three-dimensional multi-speciated aerosol distributions for the BT calculation by CRTM. The pull request (#32) of this regression test was committed and merged into the GSI master branch on GitHub on July 28, 2020.

5. Conclusion

In this DTC visitor project, we introduced a regression test into GSI to assure the functionality of accounting for aerosol effects on the BT simulation of radiance observations. To further understand the aerosol impacts on meteorological analysis, we conducted idealized CRTM experiments and standalone GSI experiments. A series of sensitivity tests were conducted to investigate the response of CRTM simulations to the presence of aerosols. The standalone experiments aimed to address the impact of aerosol-aware CRTM simulation on GSI analysis.

Idealized CRTM experiment demonstrated that aerosols have stronger impacts on BT simulation in the atmospheric window channels than other channels. In sensitivity tests of the aerosol layer properties, the BT simulations and Jacobians for layer temperature and water vapor are more sensitive to the aerosol loading and the peak concentration level than the geometric thickness of the aerosol layer and bins composition. The magnitude and vertical distribution of the Jacobians are also affected by the presence of aerosols, which would further affect the analysis increment in GSI. It is also shown that considering aerosols in the CRTM simulation will change the Jacobians of surface temperature and emissivity. Both of them are incorporated

into GSI quality control (QC) and bias correction (BC) algorithms, so the changes will affect the usage of IR observations in GSI. Further investigations on this issue may be required.

Standalone experiments reveal that considering aerosol information in the CRTM could introduce cooler simulated BTs, larger first-guess departures, and warmer atmospheric temperature analysis in the GSI system. However, it is unclear how aerosol-aware Jacobians from CRTM would affect the analysis increments in the GSI since multiple observations were assimilated. Hence, a single IR observation test is needed to quantify the impacts on analysis increment. Additionally, further studies are needed to explore how to incorporate the aerosol information properly through QC and BC in the DA system.

Acknowledgements

The author thanks DTC for facilitating the graduate student project, and is very grateful to valuable guidance from Drs. Ming Hu and Guoqing Ge. The author also thanks the input from his academic advisor, Dr. Cheng-Hsuan (Sarah) Lu, and UAlbany colleague, Dr. Dustin Grogan. The author also thanks the input from the JCSDA CRTM group, Dr. Benjamin Johnson, Dr. Patrick Stegmann, and Dr. Cheng Dang. All code development and experiments are conducted on Hera, a R&D high performance computing system (RDHPCS) at the NOAA Environmental Security Computing Center (NESCC).

References

- Chen, Y., Y. Han, and F. Weng, 2012: Comparison of two transmittance algorithms in the community radiative transfer model: Application to AVHRR, *Journal of Geophysical Research: Atmospheres*, **117**, <https://doi.org/10.1029/2011JD016656>.
- Chin, M., R. B. Rood, S.-J. Lin, J.-F. Müller, and A. M. Thompson, 2000: Atmospheric sulfur cycle simulated in the global model GOCART: Model description and global properties. *Journal of Geophysical Research: Atmospheres*, **105**, 24671–24687, <https://doi.org/10.1029/2000JD900384>.
- Colarco, P., A. da Silva, M. Chin, and T. Diehl, 2010: Online simulations of global aerosol distributions in the NASA GEOS-4 model and comparisons to satellite and ground-based aerosol optical depth. *Journal of Geophysical Research*, **115**, <https://doi.org/10.1029/2009JD012820>.

- Ding, S., P. Yang, F. Weng, Q. Liu, Y. Han, P. van Delst, J. Li, and B. Baum, 2011: Validation of the community radiative transfer model. *Journal of Quantitative Spectroscopy and Radiative Transfer*, **112**, 1050–1064, <https://doi.org/10.1016/j.jqsrt.2010.11.009>.
- Divakarla, M., and Coauthors, 2012: Evaluation of CrIMSS operational products using in-situ measurements, model analysis fields, and retrieval products from heritage algorithms. *2012 IEEE International Geoscience and Remote Sensing Symposium*, 2012, Munich, Germany, IEEE, 1046–1049.
- Eresmaa, R., J. Letertre-Danczak, C. Lupu, N. Bormann, and A. P. McNally, 2017: The assimilation of Cross-track Infrared Sounder radiances at ECMWF. *Quarterly Journal of the Royal Meteorological Society*, **143**, 3177–3188, <https://doi.org/10.1002/qj.3171>.
- Garand, L., and Coauthors, 2001: Radiance and Jacobian intercomparison of radiative transfer models applied to HIRS and AMSU channels. *Journal of Geophysical Research: Atmospheres*, **106**, 24017–24031, <https://doi.org/10.1029/2000JD000184>.
- Geer, A. J., S. Migliorini, and M. Matricardi, 2019: All-sky assimilation of infrared radiances sensitive to mid- and upper-tropospheric moisture and cloud. *Atmospheric Measurement Techniques*, **12**, 4903–4929, <https://doi.org/10.5194/amt-12-4903-2019>.
- Han, Y., P. van Delst, Q. Liu, F. Weng, B. Yan, R. Treadon, and J. Derber, 2006: JCSDA Community Radiative Transfer Model (CRTM) - Version 1. *NOAA Technical Report NESDIS*, **122**, 40 pages.
- Kim, J., S. Akella, A. M. da Silva, R. Todling, and W. McCarty, 2018: Preliminary evaluation of influence of aerosols on the simulation of brightness temperature in the NASA's Goddard Earth Observing System Atmospheric Data Assimilation System. *Technical Report Series on Global Modeling and Data Assimilation*, **49**, 44 pages.
- Letertre-Danczak, J., 2016: The use of geostationary radiance observations at ECMWF and aerosol detection for hyper-spectral infrared sounders: 1st and 2nd years report, *EUMETSAT/ECMWF Fellowship Programme Research Report*, **40**, 20 pages.
- Liang, D., and F. Weng, 2014: Evaluation of the impact of a new quality control method on assimilation of CrIS data in HWRF-GSI. *2014 IEEE Geoscience and Remote Sensing Symposium*, Quebec City, IEEE, 3778–3781.

- Liu, Q., Y. Han, P. van Delst, and F. Weng, 2007: Modeling aerosol radiance for NCEP data assimilation, in Fourier Transform Spectroscopy/ Hyperspectral Imaging and Sounding of the Environment, OSA Technical Digest Series (CD) (Optical Society of America, 2007), paper HThA5.
- Liu, Q. and C.-H. Lu, 2016: Community Radiative Transfer Model for Air Quality Studies (chapter 2), Light Scattering Reviews, Volume 11, pp 67-115, Springer Praxis Books, Springer-Verlag, Berlin – Heidelberg, 2016.
- Matricardi, M., 2005: The inclusion of aerosols and clouds in RTIASI, the ECMWF fast radiative transfer model for the infrared atmospheric sounding interferometer. *ECMWF Tech. Memo.* **474**
- Merchant, C. J., O. Embury, P. Le Borgne, and B. Bellec, 2006: Saharan dust in nighttime thermal imagery: Detection and reduction of related biases in retrieved sea surface temperature. *Remote Sensing of Environment*, **104**, 15–30, <https://doi.org/10.1016/j.rse.2006.03.007>.
- Pierangelo, C., A. Chedin, S. Heilliette, N. Jacquinet-Husson, and R. Armante, 2004: Dust altitude and infrared optical depth from AIRS. *Atmos. Chem. Phys.*, **4**, 1813-1822.
- Quan, X., H.-L. Huang, L. Zhang, E. Weisz, and X. Cao, 2013: Sensitive detection of aerosol effect on simulated IASI spectral radiance. *Journal of Quantitative Spectroscopy and Radiative Transfer*, **122**, 214–232, <https://doi.org/10.1016/j.jqsrt.2012.05.002>.
- Sokolik, I. N., 2002: The spectral radiative signature of wind-blown mineral dust: Implications for remote sensing in the thermal IR region. *Geophysical Research Letters*, **29**, 7-1-7-4, <https://doi.org/10.1029/2002GL015910>.
- Weaver, C. J., J. Joiner, and P. Ginoux, 2003: Mineral aerosol contamination of TIROS Operational Vertical Sounder (TOVS) temperature and moisture retrievals. *Journal of Geophysical Research*, **108**, <https://doi.org/10.1029/2002JD002571>.
- Weng, F., Y. Han, P. van Delst, Q. Liu, T. Kleespies, B. Yan, and J. L. Marshall, 2005: JCSDA Community Radiative Transfer Model (CRTM). *14th International TOVS Study Conference (ITSC)*, 6 pages.